Supporting Information

Basalt fibers with surface coated hybrid nanocarbon nanofillers for linear temperature and pressure sensing

Yanhua Sun, Jiaxing Guo, Yidi Hu, Muhan Chen, Lei Jing, Kai Ke*, Rui-Ying Bao, Yu Wang, Bo Yin*, Wei Yang

College of Polymer Science and Engineering, State Key Laboratory of Advanced Polymer Materials, Sichuan University, Chengdu, 610065, Sichuan, China

Corresponding authors: K. K. kaike@scu.edu.cn; B. Y. yinbo@scu.edu.cn

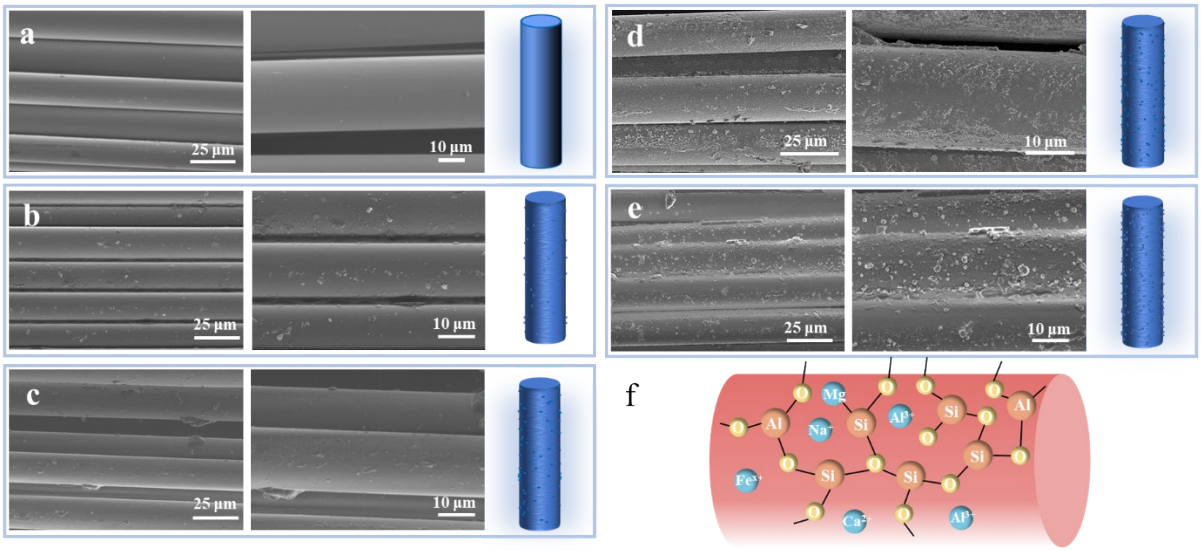

Figure S1. Surface SEM images of MBF after treatment with different concentrations of KOH solution; (a) 0 g/L, (b) 25 g/L, (c) 50 g/L, (d) 75 g/L, and (e) 100 g/L, respectively; (f) Schematic diagram of the chemical components of BF.

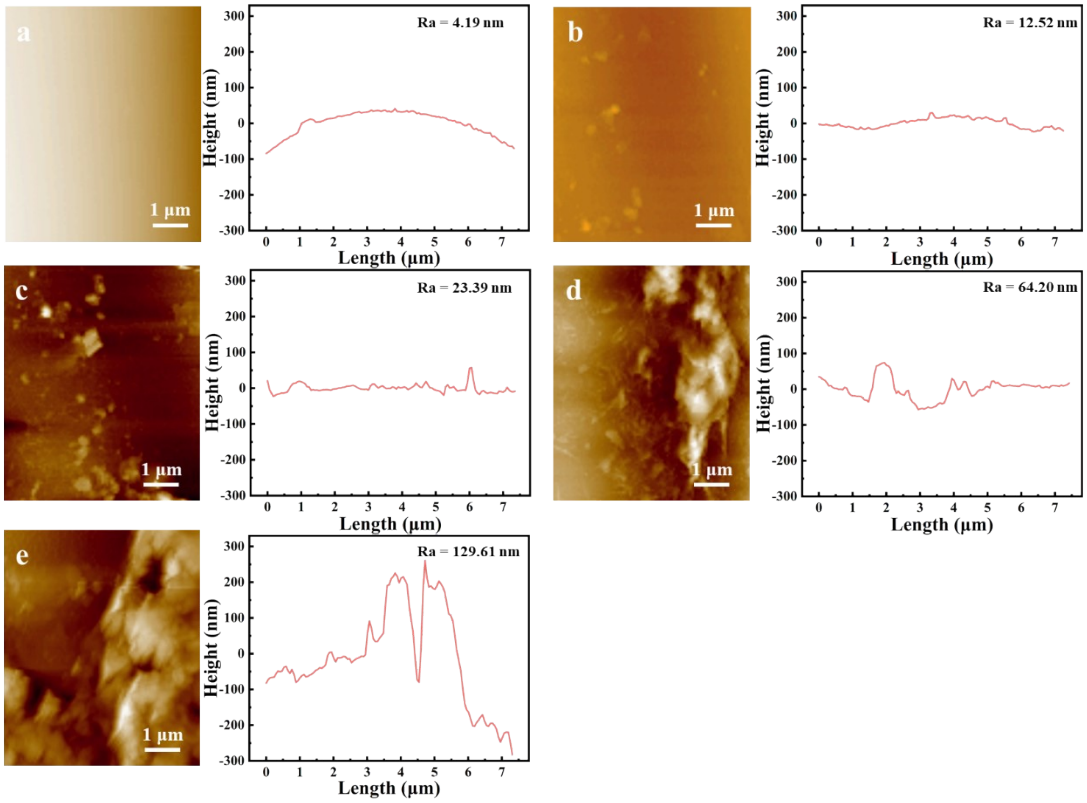

Figure S2. AFM showing the surface morphology of MBFs after KOH treatments at different KOH concentrations; (a) 0 g/L; (b) 25 g/L; (c) 50 g/L; (d) 75 g/L; and (e) 100 g/L, respectively.

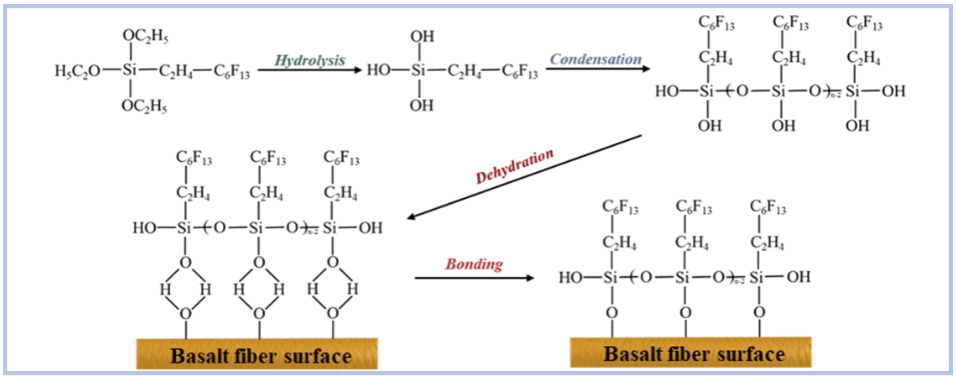

Figure S3. Schematic illustration of the grafting mechanism of the FAS-13 on BF surface.

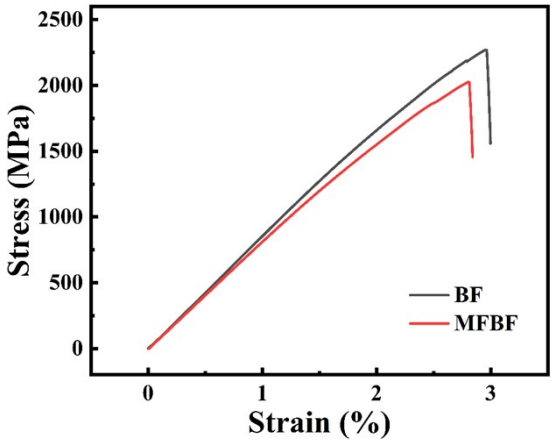

Figure S4. Tensile properties of the BF and MFBF.

Table S1. Tensile strength and elongation at break of BF and MFBF

BF	Tensile Strength (MPa)	Elongation at Break (%)	MFBF	Tensile Strength (MPa)	Elongation at Break (%)
1	2308.16	2.88	1	2048.32	2.85
2	2330.24	3.01	2	2011.57	2.79
3	2257.38	2.93	3	2059.78	2.86
4	1973.58	2.39	4	2002.19	2.78
5	2206.46	2.99	5	2033.45	2.83
6	2268.90	2.97	6	1767.12	2.35
7	2245.71	2.95	7	1995.89	2.77
8	2322.12	2.89	8	2024.21	2.81
9	1559.79	1.94	9	1986.33	2.76
10	2263.62	2.92	10	2041.67	2.84
Mean ± SD	2275.32 ± 42.09	2.94 ± 0.05	Mean ± SD	2023.01 ±25.29	2.81 ±0.04

Noting: Samples 4, 9 of BF, and 6 of MFBF were excluded from statistical analysis as they exhibited non-representative fracture modes (e.g., fracture at the grip).

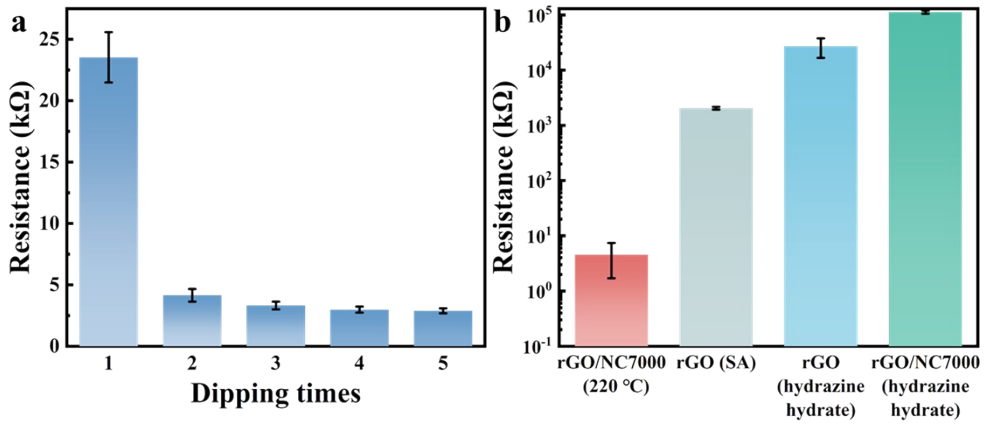

Figure S5. Initial resistance of the MFBFs (a) impregnated in GO/NC7000 slurry for different times and (b) with different fabrication methods.

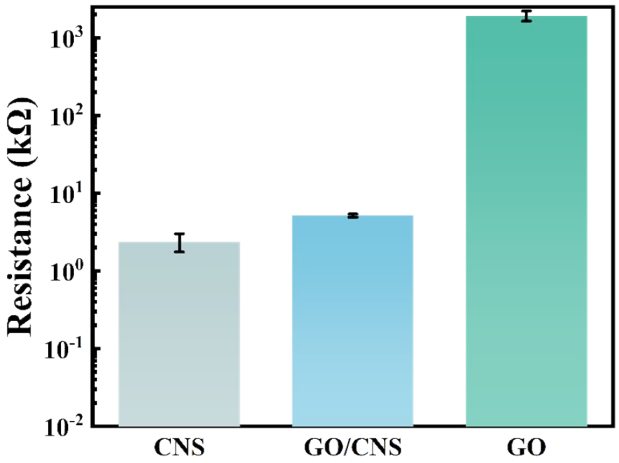

Figure S6. Initial electrical resistance of the MFBFs coated with different carbon nanomaterials.

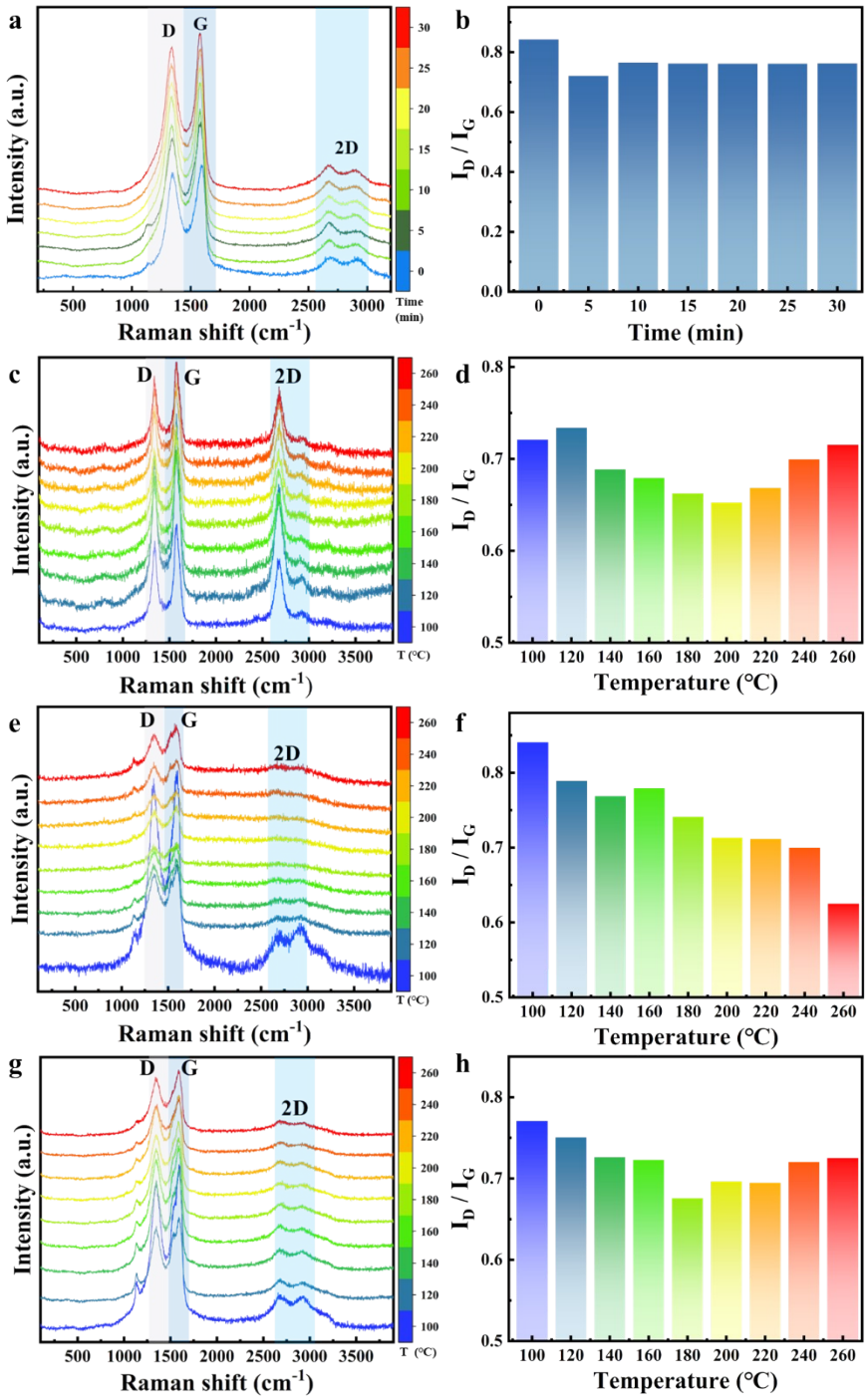

Figure S7. (a, b) In-situ Raman test spectra and I_D/I_G value changes of the MFBFGC at 250 ℃; Changes in in-situ Raman spectra and the I_D/I_G ratio of (c, d) the MFBFC, (e, f) the MFBFG and (g, h) the MFBFCG with an increasing temperature.

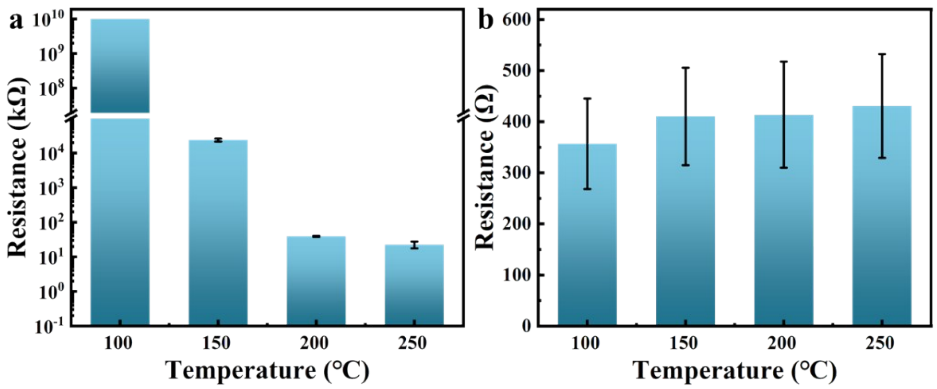

Figure S8. Initial resistance of (a) the MFBFG and (b) the MFBFC after thermal treatment at 100 ℃, 150 ℃, 200 ℃, and 250 ℃.

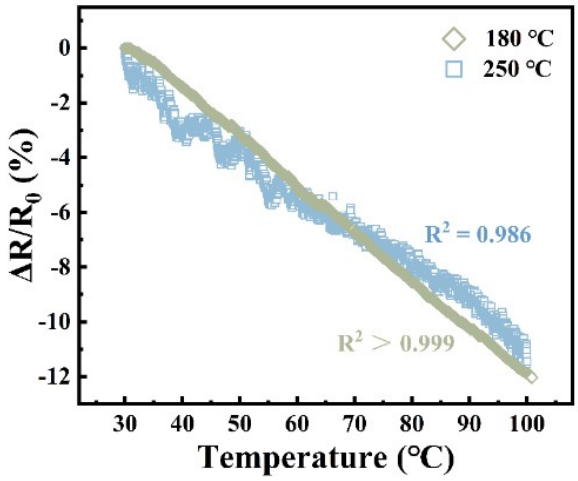

Figure S9. Relative resistance change versus temperature for the MFBFCG annealed at180 °C and 250 °C at a heating rate of 10 ℃/min within a temperature range of 30-100 ℃.

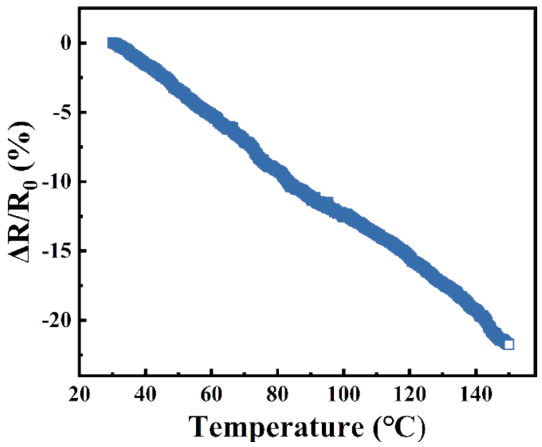

Figure S10. $\Delta R/R_0$-temperature curve of the MFBFCG within 30 ℃-150 ℃ at a heating rate of 3 ℃/min.

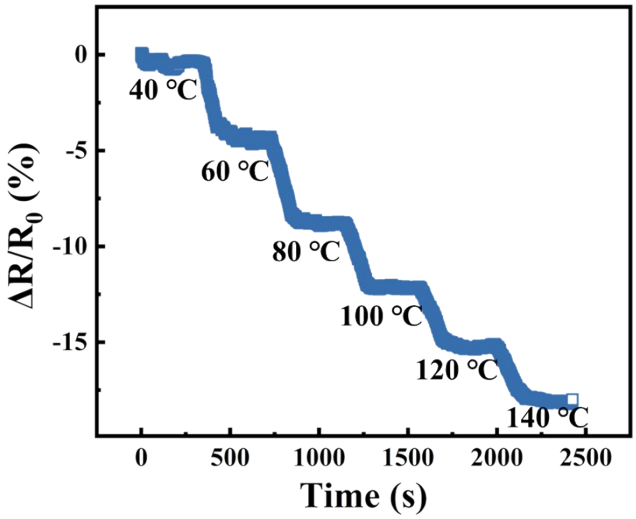

Figure S11.The change of $\Delta R/R_0$ of the MFBFCG under stepwise temperature changes from 40 ℃ to 140 ℃ with an interval of 20 ℃ at a heating rate of 3 ℃/min.

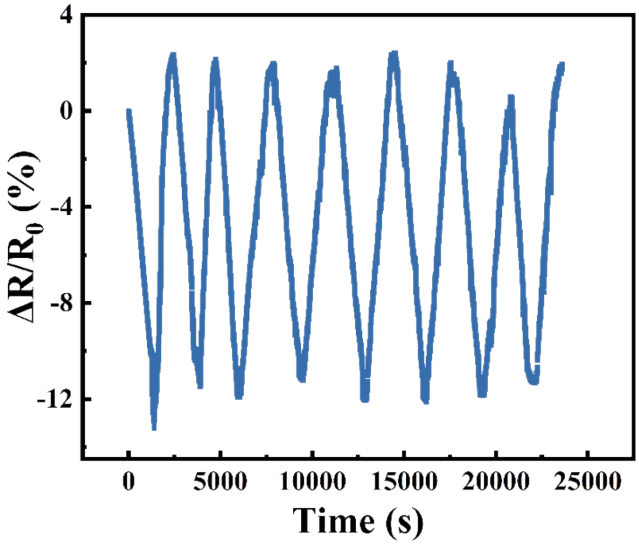

Figure S12. $\Delta R/R_0$ of the MFBFCG during temperature cycling from 30 ℃ to 100 ℃ at a heating rate of 3 ℃/min.

Table S2. Quantitative Analysis of Atomic Chemical Composition of BFs.

Sample	Chemical composition (%)								
	C	O	F	Si	Al	C/Al	O/Al	F/Al	Si/Al
MBF	59.95	26.07	5.95	5.98	2.06	29.10	12.66	2.89	2.90
MFBF	27.93	6.56	61.70	3.42	0.40	69.83	16.40	154.25	8.55

Table S3. Initial resistance of the MFBFCG, the MFBFC and the MFBFG.

Sample	Initial resistance (kΩ)			
	100 ℃	**150 ℃**	**200 ℃**	**250 ℃**
MFBFCG	4.89	3.60	1.08	0.91
MFBFC	0.36	0.41	0.41	0.43
MFBFG	-	23933.33	39.08	22.53

Table S4. A comparison of electrical conductivity and tensile strength of the recently reported composites based on BF.

Material	Conductivity (S/m)	Mechanical strength	Ref.
BF/MWCNT/epoxy	10^{-4}	High	1
BF/CNT	53.0	High	2
BF/ANF/CNT	1430.0	Low	3
GF-BD	3.2×10^{4}	Low	4
Gr/PVDF/SEBS	$(1.4\pm1.0)\times10^{-3}$	Low	5
PVA-HEC hydrogel	5.8	Low	6
Au/MXene/CNT/PU	4772.0	Low	7
BGCP/CNT/PEN	7.0×10^{-4}	Low	8
MFBFCG	**230**	**High**	**This work**

Noting: Here the mechanical strength is classified as high (≥ 800 MPa), moderate (400-800 MPa) and low (< 400 MPa).

1. D. Quan, et al., Synergistic Toughening and Electrical Functionalization of an Epoxy Using MWCNTs and Silane-/Plasma-Activated Basalt Fibers, *J. Appl. Polym. Sci.*, 2021, **138**, 49605, DOI: 10.1002/app.49605.
2. D. Xing, et al., Thermoelectric Performance of Basalt Fiber with Nanocomposite Sizing, *Colloids Surf. A*, 2023, **672**, 131761, DOI: 10.1016/j.colsurfa.2023.131761.
3. S. Song, et al., Flexible Basalt Fiber/Aramid Nanofiber/Carbon Nanotube Electromagnetic Shielding Paper with Outstanding Environmental Stability and Joule Heating Performance, *ACS Appl. Mater. Interfaces*, 2023, **15**, 35495-35506, DOI: 10.1021/acsami.3c06138.
4. Y. Zhi, et al., High-Performance Pressure Sensors Based on Graphene Fibers with

Bilateral Dense Structures for Human Motion Monitoring, *J. Mater. Sci. Technol.*, 2026, **259**, 209-219, DOI: 10.1016/j.jmst.2025.07.057.

5. A. Fatima, et al., Tunable Conductivity and Porosity in Nanocomposite Fibers for Multimodal Wearable Sensing, *Adv. Compos. Hybrid Mater.*, 2026, **9**, 75, DOI: 10.1007/s42114-025-01614-5.
6. X. Wang, et al., High-Strength, Highly Conductive and Woven Organic Hydrogel Fibers for Flexible Electronics, *Chem. Eng. J.*, 2022, **428**, 131172, DOI: 10.1016/j.cej.2021.131172.
7. L. Lan, et al., A Stretchable and Conductive Fiber for Multifunctional Sensing and Energy Harvesting, *Nano Energy*, 2021, **84**, 105954, DOI: 10.1016/j.nanoen.2021.105954.
8. L. Liu, et al., Hierarchically Structured Basalt Fiber Reinforced Poly (Arylene Ether Nitrile) Composites for Enhanced Mechanical, Electrical, and Damage Self-Sensing Performance, *Compos. Sci. Technol.*, 2025, 111359, DOI: 10.1016/j.compscitech.2025.111359.